The British Journal of Radiology, 84 (2011), 677–690

REVIEW ARTICLE

Malignant tumours of the small intestine: a review of histopathology, multidetector CT and MRI aspects

M ANZIDEI, PhD, A NAPOLI, MD, PhD, C ZINI, MD, M A KIRCHIN, MD, C CATALANO, MD and R PASSARIELLO, MD

Department of Radiological Sciences, ''Sapienza'' University of Rome, Rome, Italy

ABSTRACT. Small bowel neoplasms, including adenocarcinoma, carcinoid tumour, lymphoma and gastrointestinal stromal tumours, represent a small percentage of gastrointestinal cancers, yet are among those with the poorest prognosis compared with other gastrointestinal malignancies. Unclear clinical scenarios and difficult radiological diagnosis often delay treatment with negative effects on patient survival. Recently, multidetector CT (MDCT) and MRI have been introduced as feasible and accurate diagnostic techniques for the identification and staging of small bowel neoplasms. These techniques are gradually replacing conventional barium radiography as the tool of choice. However, the inherent technical and physiological challenges of small bowel imaging require a familiarity with patient preparation and scan protocols. Adequate knowledge of the histopathology and natural evolution of small bowel neoplasms is also important for differential diagnosis. The aim of this article is to review MDCT and MRI protocols for the evaluation of small bowel tumours and to provide a concise yet comprehensive guide to the most relevant imaging features relative to histopathology.

Received 10 August 2010
Revised 14 October 2010
Accepted 2 November 2010

DOI: 10.1259/bjr/20673379

The small intestine (SI) accounts for 75% of the length and 90% of the mucosal surface of the alimentary tract; however, because of certain unique physiological features (rapid transit, alkaline content, IgA secretion and lymphoid tissue) it is the site of only 2–6% of all gastrointestinal (GI) neoplasms [1, 2]. Data from the United State Surveillance Epidemiology and End Results (SEER) programme from 2002 to 2006 [3] show an age-adjusted incidence rate for malignant tumours of 1.9 per 100 000 men and women per year with an age-adjusted death rate of 0.4 per 100 000 men and women per year. Apart from obscure GI bleeding, patients may present with non-specific complaints such as abdominal pain (60%), anaemia (50%), nausea and vomiting (50%), weight loss (40%), diarrhoea (30%) and intestinal obstruction (30%) [4]. However, many patients may remain asymptomatic until the late stages of disease. SI neoplasms are also difficult to identify at diagnostic imaging and as a result delays in diagnosis are common. Maglinte et al [5] estimated that while delays in diagnosis of less than 2 months were common because the patient failed to report symptoms, extended delays occurred as a result of the physician not ordering the appropriate examinations (>8 months) and/or because the radiologist failed to make the correct diagnosis (approximately 12 months). An unfortunate consequence of late diagnosis is poor prognosis [3]. 5 year survival rates range from 0–28% for adenocarcinoma, 14–30% for lymphoma and 60% for carcinoid tumours.

Until recently, barium enteroclysis has been considered the most accurate radiological modality to detect small bowel malignancies [6]. However, this technique requires duodenal intubation and direct injection of barium and methylcellulose into the intestinal lumen and is both time-consuming and poorly tolerated by patients. Furthermore, barium enteroclysis is limited in its ability to accurately depict the mural and extramural extent of disease [6]. Alternatives to barium enteroclysis for imaging the SI are multidetector CT (MDCT) and MRI. Both techniques have good potential for the early diagnosis of both inflammatory and neoplastic conditions. The aims of this review are to present MDCT and MRI protocols for SI imaging, to describe the typical imaging features of common SI neoplasms and to correlate radiological findings with specific histopathological characteristics.

Imaging techniques

Patient preparation

MDCT

The patient should fast on the day of the examination to reduce alimentary residue in the GI tract, which may lead to inhomogeneous intraluminal attenuation.

Address correspondence to: Dr Michele Anzidei, Department of Radiological Sciences, University of Rome ''La Sapienza'', Viale Regina Elena 324, 00161, Rome, Italy. E-mail: michele.anzidei@gmail.com

Because the SI can be partly or fully collapsed under normal physiological conditions, luminal distension is a necessary pre-requisite for imaging because collapsed bowel loops can hide even large lesions or mimic wall thickening. Whereas both MRI [7] and MDCT enteroclysis [8] allow optimal lumen distension, oral administration of contrast agent with the proper choice of oral contrast material and adequate timing can produce good results [9, 10], is more patient-friendly and less time consuming. For MDCT, the choice of oral contrast agent is usually determined by the anatomical SI region of interest and the clinical question to be answered (Figure 1). While water is often a good option to distend the duodenum and the proximal tract of the jejunum (1–1.5 l of tap water given 10–15 min before examination, with the last 2–3 glasses drunk in the CT room) [11], imaging of the distal jejunum and/or ileum requires a different approach, since water is rapidly absorbed by the intestinal wall during its transit through the lumen. For these regions, a low-concentration contrast agent with bland osmotic activity represents the best compromise between bowel distension and lumen attenuation. Such contrast mixtures (*e.g.* water, sorbitol and 0.1% barium sulphate) typically require fractioned administration over a period of 50–65 min before the examination [12]. Highly concentrated barium or iodine solutions must be avoided because too high an intraluminal attenuation can jeopardise the identification of small hypervascular masses (*i.e.* carcinoid tumours) or compromise the evaluation of mesenteric vessels [13, 14]. The use of peristalsis inhibitors such hyoscine *N*-butyl bromide (HBB, Buscopan Boehringer Ingelheim GmbH, Ingelheim am Rhein, Germany) is strongly recommended (intravenous administration after completing intestinal preparation) in order to prolong lumen distension and avoid movement artefacts.

MRI

The dietary recommendations are similar to those for MDCT. Oral contrast agents for MRI can be classified as positive, negative or biphasic according to their action on the signal intensity of bowel lumen [15] (Figure 2). Positive contrast agents are paramagnetic, *i.e.* water-based gadolinium (Gd) solutions that produce high-signal intensity (the so-called ''luminographic'' effect) on both T_1 and T_2 weighted sequences [16]. The main limitations of this approach are the relative high cost and the fact that wall enhancement after intravenous Gd administration can be masked by the higher lumen signal on T_1 weighted sequences [17]. Negative contrast agents are superparamagnetic, *i.e.* water-based solutions of iron oxide particles coated with silicone that produce low-signal intensity (the so-called ''dark-lumen'' effect) on both T_1 and T_2 weighted sequences [16]. Although these agents often permit better visualisation of bowel wall and mesenteric fat oedema on T_2 weighted sequences [18, 19], magnetic susceptibility artefacts that affect image quality may occur on gradient-echo sequences. Biphasic contrast agents are water solutions of hyperosmotic compounds (*i.e.* polyethelenglycol) that produce both the luminographic effect on T_2 weighted sequences and the dark lumen appearance on T_1 weighted sequences [16]. Biphasic agents represent the most flexible solution, with the advantage of cost containment [20, 21]. MR-enteroclysis with naso-jejunal intubation and 1500–3000 ml of contrast agent (administered at 80–150 ml min^{-1} using infusion pumps) has proven to be highly effective for the detection of inflammatory bowel diseases and SI cancers [7]. However, in most patients adequate intestinal distension can be obtained with a conventional per os preparation (600 ml to 1 l of tap water with polyethelenglycol for 20–30 min before the examination). Moreover, since there is no radiation exposure, bowel distension can be monitored dynamically and adjusted during the examination [15]. Once sufficient bowel distension is achieved, peristalsis inhibitors may be used to suppress motility induced artefacts that can produce proton dephasation inside the lumen, mimicking filling defects on T_2 weighted images.

(a) (b) (c)

Figure 1. Different oral contrast agents for multidetector CT of the small intestine (SI). (a) Tap water is an easy and inexpensive way to distend the SI. Water is frequently used to better visualise the superior portion of GI tract (stomach and duodenum); however, it is rapidly absorbed during its passage through the jejunum and ileum with a progressive loss of bowel distension in the distal tract. (b) High-concentration opaque oral contrast agents present a low absorption rate and remain in the bowel for a long time; however, their high attenuation characteristics may not allow an accurate evaluation of the intestinal lumen or enhancement of the bowel walls. (c) Low-concentration oral contrast agents provide excellent distension of the bowel lumen owing to moderate osmotic pressure, maintaining at the same time an adequate attenuation gradient between wall and lumen.

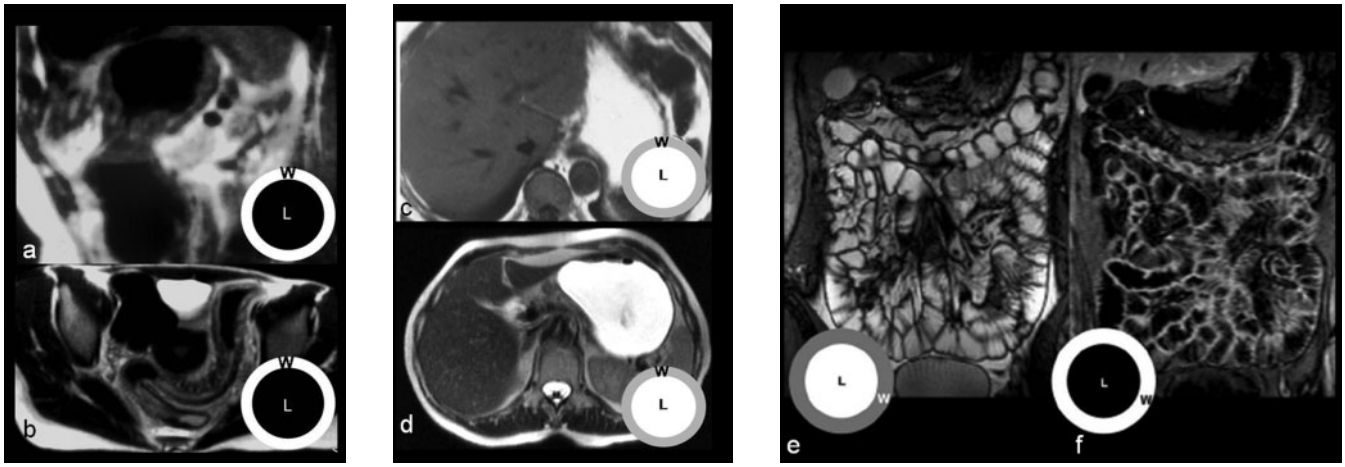

Figure 2. Different oral contrast agents in MRI of the small intestine (SI). Double-negative contrast agents produce low-signal intensity of bowel lumen on both (a) T_1 and (b) T_2 weighted sequences. With these contrast agents the visualisation of the bowel's wall (w) is preferred to that of the lumen (l), emphasising the identification of parietal and extra-parietal findings such as oedema or fat stranding. With the use of positive contrast agents, the visualisation of bowel lumen is privileged on both (c) T_1 and (d) T_2 weighted sequences; the most significant limitation is represented by the fact that wall enhancement after intravenous Gd administration can be masked by the higher lumen signal on T_1 weighted sequences. Biphasic contrast agents produce an optimal contrast between lumen and walls on both (e) T_2 weighted (bright lumen and dark walls) and (f) T_1 weighted sequences (dark lumen and bright walls).

Imaging protocol

MDCT

A preliminary unenhanced acquisition of the whole abdomen from the dome of the diaphragm to the pelvis is recommended in order to properly detect mesenteric calcifications or intraluminal bleeding and for the imaging of liver parenchyma if a malignancy is suspected. Thereafter, depending on the indication, arterial and/or portal venous phase imaging [14, 22] must be performed after intravenous administration of contrast agent (2 ml kg^{-1} at 3.5–4 ml s^{-1}). Bolus tracking techniques with measurements performed in the abdominal aorta can be used to adapt the delay between contrast agent administration and scan initiation to the cardiac output of the individual patient; however, delays of 35–40 s and 60–65 s are often appropriate for arterial and portal-venous phase acquisitions, respectively. Arterial phase imaging is recommended when a strongly enhancing lesion (*e.g.* neuroendocrine tumours or metastases from melanoma) is suspected. When using a 4-slice scanner, a collimation of 4 × 2.5 mm should be

Table 1. Epidemiology and demographics of small intestine neoplasms

Histology	Incidence per year	m/f ratio	Risk factors	5 year survival rate
Adenocarcinoma	Overall=0.4 per 100 000 Wm=30.8% Wf=32.7% Bm=37.2% Bf=45.5%	W m/f=1.5 B m/f=1.2	Crohn disease, coeliac disease, familiary adenomatous polyposis, Meckel diverticulum	26.6–39%
Carcinoid	Overall=0.4 per 100 000 Wm=36.0% Wf=39.2% Bm=43.9% Bf=39.7%	W m/f=1.4 B m/f=1.6	MEN1	60–76.5%
Lymphoma	Overall=0.3 per 100 000 Wm=22.9% Bm=11.4% Wf=17.9% Bf=7.3%	W m/f=1.9 B m/f=2.3	EBV, AIDS (B cell) Coeliac disease (T cell) Chemotherapy	8–25%
GIST	Overall=0.2 per 100 000 Wm=10.3% Bm=7.4% Wf=10.2% Bf=7.5%	W m/f=1.4 B m/f=1.4	No	45–55%
Metastases	Autopsy series: Lung cancer (12%) Breast cancer (16%) Melanoma (42%)		Lung cancer Melanoma Breast cancer	End stage of disease, resection of solitary lesions may prolong survival

W, white; B, black; m, male; f, female; EBV, Epstein-Barr virus; AIDS, acquired immune deficiency syndrome; GIST, gastrointestinal stromal tumour.

(a) (b)

Figure 3. Adenocarcinoma. (a) Photograph of resected and opened duodenum from a 67-year-old man who presented with melaena shows a 2.0 cm vegetating lesion originating from the mucosa surrounding the duodenal papilla. (b) Low-power photomicrograph (magnification ×4; haematoxylin–eosin stain) of the lesion shows neoplastic infiltration (asterisk) of the mucosal epithelium and muscularis propria.

considered the minimum setting to reconstruct 3 mm slices. Conversely, a collimation of 4 × 1 mm allows 1.25 mm slice reconstruction that can be adapted to image mesenteric vessels, but at the cost of a longer scan duration, which may exceed the breath-hold capability of frail patients. The availability of faster scanners permits the routine use of submillimetre collimations (16 × 0.75 mm and 64 × 0.75 mm) that can generate almost isotropic three-dimensional (3D) data sets from multiphasic acquisitions. Evaluation of MDCT data sets should be performed on off-line consoles dedicated for 3D reconstructions (the availability of maximum intensity projection and multiplanar reformatted images facilitates the evaluation of SB lumen and its relationship with adjacent vessels) [14, 22].

MRI

The effects of breathing artefacts and bowel wall motion during data acquisition are the main causes of image degradation and poor diagnostic accuracy in MRI of the SI. For this reason later generation MRI scanners operating at 1.5–3 T are preferable while parallel imaging protocols and fast sequences are mandatory. Regarding acquisition geometry, the coronal plane optimally demonstrates the anatomy of the SI, mesentery and abdominal vessels, but additional axial and sagittal planes should also be considered for precise evaluation of the SI and to avoid problems with partial volume effects. According to most literature reports, there are three types of sequence that must be included in a complete MRI protocol for SI imaging:

Table 2. Summary of typical and atypical imaging findings of small intestine neoplasms

Histology	Typical appearance	Atypical appearance
Adenocarcinoma	Concentric lumen narrowing with irregular edges	Polypoid lesions with well-defined surface and margins
	Complete bowel obstruction	Central ulcerations
	Heterogenous enhancement	Duodenal localisation
Carcinoid	Small (<2 cm) single or multiple filling defects	Ill-defined thickening of bowel wall without discrete mass
	Desmoplastic reaction of the mesentery	Absence of desmoplastic reaction
	Hypervascular	Duodenal or jejunal localisation
Lymphoma	Coarse segmental wall thickening with ulceration and necrosis	Discrete polyp that may be a lead point of intussusception
	Bulky lymphyadenopathies	Absence of significant lymphoadenopathies
	Aneurysmal dilatation of bowel loops	No signs of bowel occlusion
GIST	Large regular mass with inhomogeneous enhancement	Irregular mass with low attenuation and poor enhancement
	Necrosis and/or ulceration	Larger calcifications
	Ileal localisation	Direct vascular encasement
Metastases	Intraluminal nodules develeloping from haematogenous spread to submucosal layers	Large serosal masses developed from intraperitoneal seeding from gastrointestinal cancers

GIST, gastrointestinal stromal tumour.

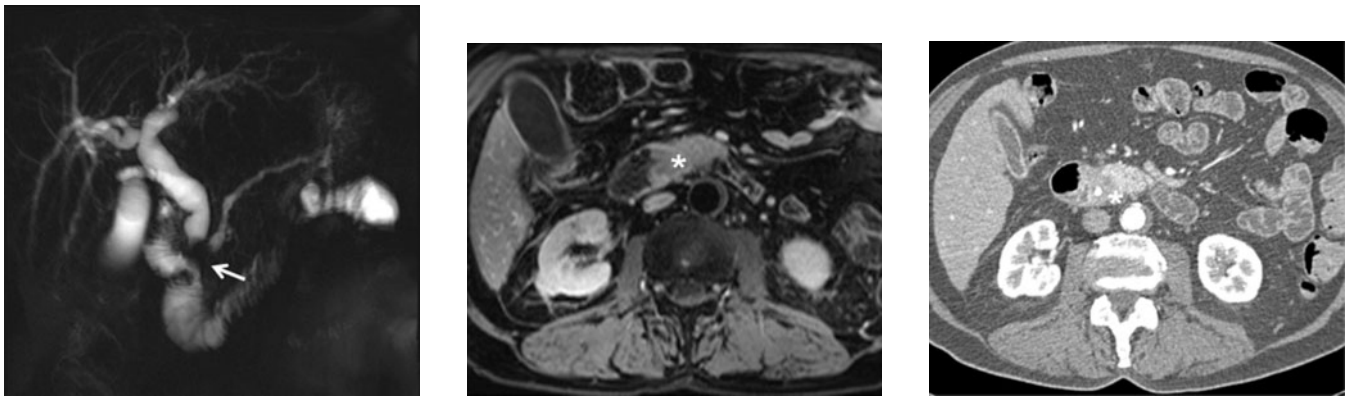

(a) (b) (c)

Figure 4. Adenocarcinoma. Same patient as Figure 3. (a) Magnetic resonance cholangiopancreatography (MRCP) demonstrates obstruction of the main pancreatic duct and common bile duct with signal loss at the duodenal papilla (arrow), stasis and dilatation of the hepatic biliary branches. (b) Fat-suppressed axial T_1 spoiled gradient-echo (SPGRE) sequences obtained after intravenous administration of contrast agent and water distension of the duodenum allowed identification of a hypervascular protrusion from the papilla (asterisk). (c) Multidetector CT performed after biliary stenting confirm the presence of the lesion (asterisk) that can be clearly differentiated from the pancreatic parenchyma, excluding, at the same time, infiltration of the perivisceral fat tissue.

- The main advantage of T_2 weighted fast spin-echo sequences, or turbo spin-echo (TSE) acquisitions, is the excellent soft-tissue contrast, which permits detection of diseased bowel segments and evaluation of the surrounding mesentery [23, 24]. The use of half-Fourier acquisition single-shot turbo spin-echo (HASTE) technique increases the speed of acquisition resulting in reduced or absent movement artefacts [25]. On the other hand, these sequences are susceptible to flow-related artefacts (owing to the long echo time (TE)) and thus rapid peristaltic movements may result in intraluminal flow voids that may be perceived as pseudolesions.
- True fast imaging with steady-state precession (true-FISP) sequences are fully balanced gradient-echo sequences and provide the highest signal among steady-state sequences. Contrast is a function of T_1/T_2. If short repetition time (TR) and TE are used the T_1 portion remains constant and the images are mainly T_2 weighted, with bowel lumen appearing hyperintense. The speed and motion insensitivity of the acquisition completely eliminates breathing or peristalsis induced artefacts [17, 26]. Unlike the half-Fourier technique, intraluminal flow voids do not affect steady-state precession sequences; moreover, selective fat-suppression pulses can be used to

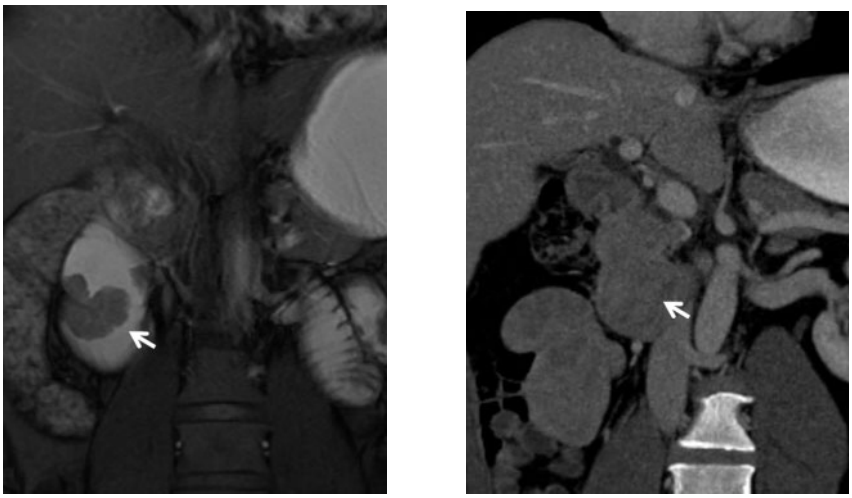

(a) (b)

Figure 5. Adenocarcinoma. 49-year-old male with melaena and endoscopic diagnosis of duodenal mass. The high intraluminal signal achieved on (a) MR true fast imaging with steady-state precession (true-FISP) image after water distension of the duodenum allows the identification of a polypoid lesion (arrow) with a thick stalk and lobulated profiles facing the duodenal papilla. The contour of the outer wall layers is preserved, excluding deep extraluminal infiltration. (b) In this case, the poor attenuation gradient and lesser lumen distension attained on multidetector CT prevent a precise delineation of the lesion (arrow).

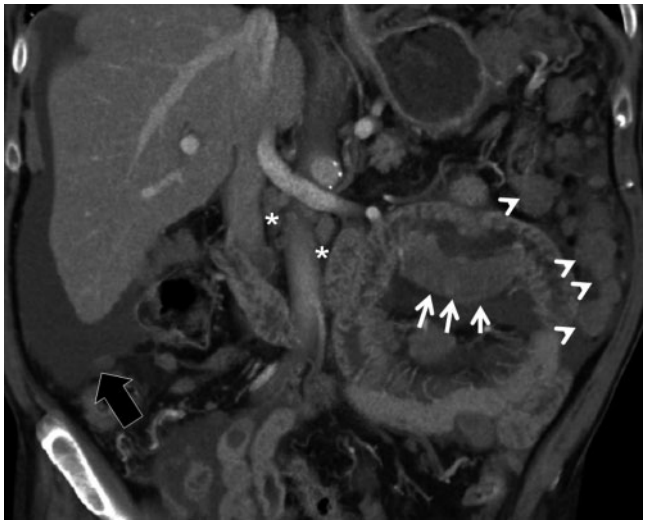

Figure 6. Adenocarcinoma. 89-year-old male with weight loss, abdominal pain and melaena admitted to the emergency room. Multidetector CT images obtained after oral administration of a low-concentration contrast agent demonstrate an eccentric and partially stenosing wall thickening involving one of the proximal jejunal loops (arrows). The lesion extends beyond the wall infiltrating the perivisceral fat. Multiple peritoneal implants (arrowheads), perihepatic ascites (black arrow) and some centimetric lymphadenopaties (asterisk) are also visualised.

increase the luminographic effect and remove ''black boundary'' artefacts caused by magnetic susceptibility [27, 28].

- T_1 weighted spoiled gradient-echo (SPGRE) sequences with fat suppression are sequences that use a semi-random spoiler gradient after each echo to spoil the remaining transverse magnetisation. These T_1 weighted sequences can be acquired as two dimensional (fewer motion artefacts) or 3D (higher spatial resolution) data sets. Their use after intravenous Gd administration permits excellent depiction of the mesenteric vessels and identification of hypervascular bowel walls if coupled with a selective spectral fat-suppression pulse [27, 29, 30].

Histopathology and imaging findings

Adenocarcinoma

Adenocarcinoma is the most common primary malignancy of the SI and accounts for 40% of cancers (Table 1). The predominant location of adenocarcinoma is the duodenum and proximal jejunum, with the incidence decreasing distally [31]. The exception to this presentation is seen in Crohn's disease, where most adenocarcinomas occur in the ileum. Adenocarcinomas may be polypoid, infiltrating or stenosing [32]. Duodenal adenocarcinomas are usually more circumscribed with a polypoid or protuberant appearance (Figure 3). Conversely, jejunal or ileal lesions tend to be larger, annular, constricting tumours with circumferential involvement of the intestine wall; at the time of diagnosis most show a fully parietal penetration and involvement of the serosal surface [33] (Table 2). An increased incidence of small bowel adenocarcinoma has been described in patients affected by familiary adenomatous polyposis (mainly periampullary) and Lynch syndrome. Small bowel

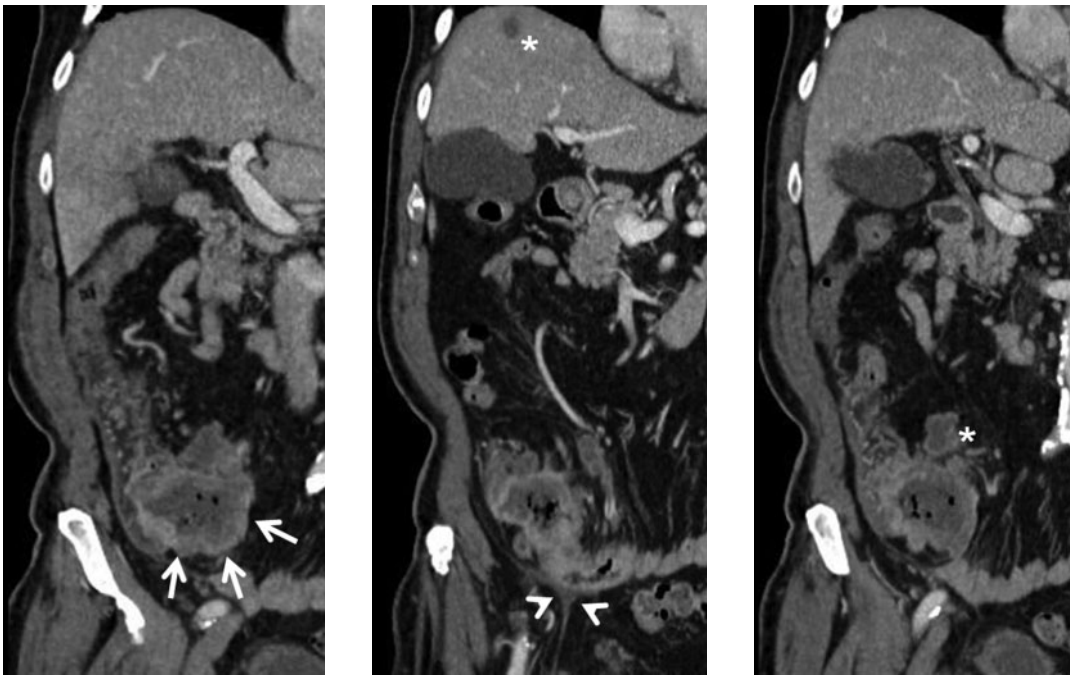

(a) (b) (c)

Figure 7. Adenocarcinoma. 66-year-old male with weight loss, melaena and incomplete colonoscopy. Multidetector CT images demonstrate a large mass originating from the last ileal loop ((a) arrows) infiltrating the ileocaecal valve. The lesion extends into the perivisceral fat and infiltrates the peritoneum ((b) arrowheads). A small liver metastasis ((b) asterisk) and necrotic lymphadenopaties ((c) asterisk) can also be identified.

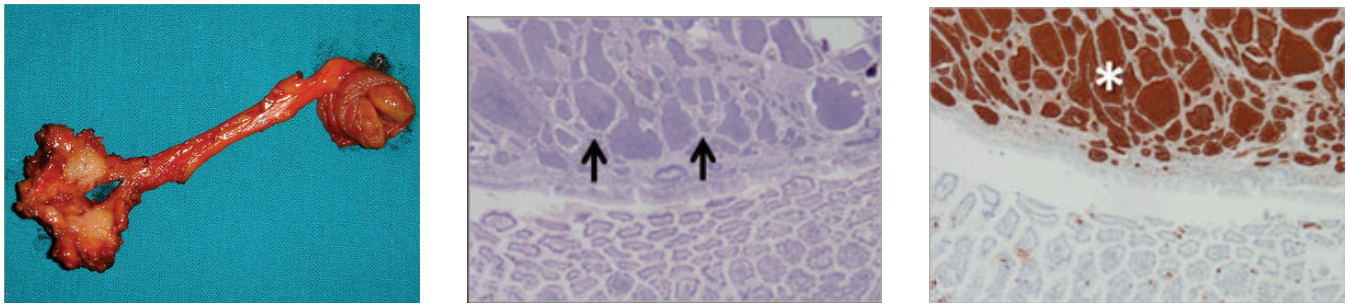

(a) (b) (c)

Figure 8. Carcinoid tumour. (a) Photograph of resected and opened jejunal loop (on the right) and mesentery (on the left) from a 57-year-old woman who presented with diarrhoea, flushing and abdominal pain shows a 1.5 cm rounded lesion originating from the jejunal wall without mucosal effacement and stranding of the mesentery ending in a plaque-like area of desmoplastic reaction. (b) Low-power photomicrograph (magnification ×4; haematoxylin–eosin stain) of the lesion shows neoplastic involvement of the submucosal layer extensively with transmural extension (arrows). There is no neoplastic change of surface epithelium. (c) Cromogranin antibodies stain confirms the diagnosis of carcinoid tumour (asterisk).

carcinomas resemble their counterparts in the colon, but with a higher proportion of poorly differentiated tumours with glandular, squamous and undifferentiated neuroendocrine components [34].

At imaging duodenal carcinomas often appear as polypoid, well-delineated lesions [35, 36] (Figures 4 and 5), although high-grade cancers may show more aggressive behaviour. Central ulceration may be present in 10% of cases. Adenocarcinomas of the jejunum and ileum usually appear as an annular narrowing with abrupt concentric or irregular ''overhanging edge'' stenosis (Figure 6) that could lead to partial or complete obstruction [17, 22]. After intravenous contrast agent administration, moderate heterogeneous enhancement is usually seen [14]. Extraluminal infiltration may appear as fat stranding on MDCT and hyperintensity of the outer wall layers and fat on T_2 weighted fat suppressed MR sequences. Adenocarcinoma of the ileum may mimic Crohn's disease for its clinical and radiological features; however, in our experience the absence of significant engorgement of the *vasa recta* (the ''comb'' sign in Crohn's disease) and the presence of a single focal lesion rather than multiple ''skip'' areas of wall thickening may be useful criteria to suspect malignancy (Figure 7). Secondary lymphadenopathies may be present at the time of diagnosis and must be differentiated from the bulkier nodes that occur when there is lymphomatous involvement of the mesentery.

Carcinoid tumours

Carcinoid is the second most common malignancy, accounting for approximately 20–25% of all SI lesions, although its frequency has been recently reported to be increased up to 35%. These tumours arise from enterochromaffin cells situated in the crypts of Lieberkühn and produce serotonin and other histamine-like

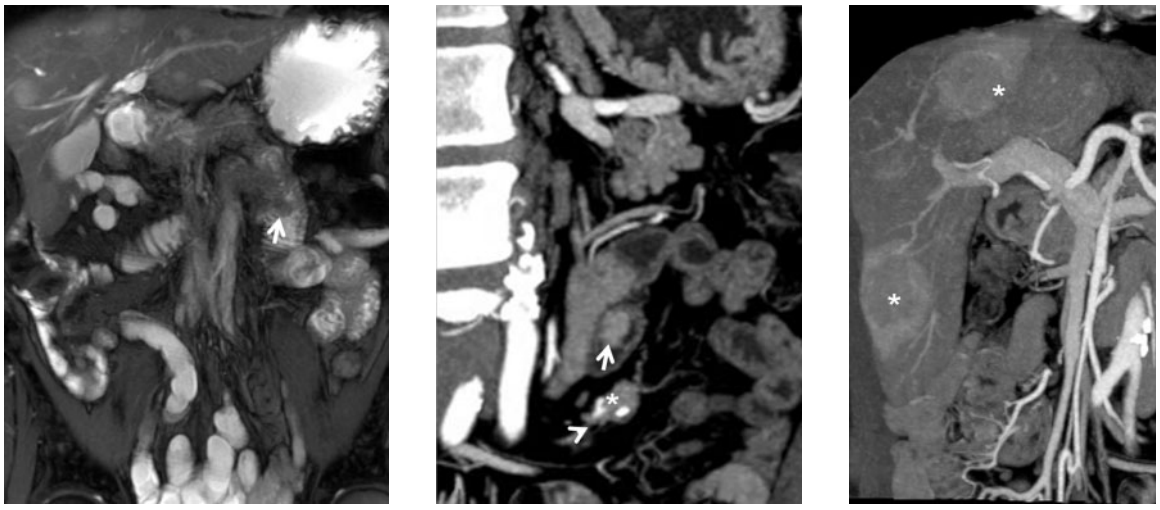

(a) (b) (c)

Figure 9. Carcinoid tumour. Same patient as Figure 8. (a) Coronal true fast imaging with steady-state precession (true-FISP) image demonstrates a small filling defect (arrow) in the first jejunal loop; some liver lesions can also be visualised. (b) Multidetector CT image obtained in the same patient in the arterial phase show a small intraluminal enhancing lesion (arrow) and mass forming desmoplastic alteration of the mesentery (arrowhead) with punctate calcifications (asterisk). (c) The portal-venous scan also shows multiple hypervascular liver metastases (asterisk).

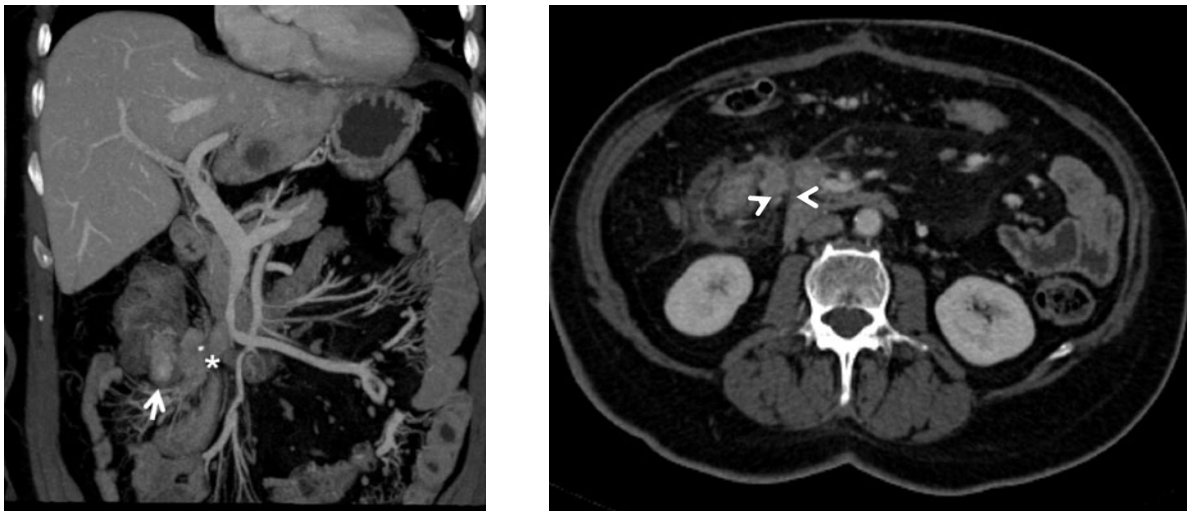

(a) (b)

Figure 10. Carcinoid tumour. 50-year-old male with multiple liver lesions identified at a routine ultrasound scan from an unknown primary cancer. (a) Multidetector CT images obtained in the portal-venous phase demonstrate an enhancing ileal lesion (arrow) with mass forming desmoplastic reaction in the mesentery (asterisk) the prominent mesenteric involvement is well visualised on the axial images ((b) arrowheads).

substances [37]. Carcinoid tumours are more common in the ileum (most within 60 cm of the ileocecal valve) than in the jejunum or duodenum, and lesions may be multiple and/or metastatic (liver and lungs) at the time of diagnosis. Prognosis is usually negatively related to the age of the patient and the size of tumour. Macroscopically carcinoid presents as an intramural or mucosal mass that may infiltrate the mesentery causing a strong desmoplastic reaction that results in calcification, fat stranding and eventually kinking of the bowel segments (Figure 8), often with intestinal obstruction [38]. Histologically, the tumours resemble adenocarcinomas, but with a less aggressive evolution. SI lesions show a strong argentaffin reaction and immunohistochemical staining (chromogranin, neuron specific enolase, sinaptophysin) is mandatory in order to confirm the histological classification (Figure 8).

At diagnostic imaging carcinoid usually appears as a parietal nodule with avid contrast enhancement in the arterial phase [14, 17, 22] (Figure 9). Since most lesions are small (<2 cm) at the time of the examination, optimal distension of the bowel lumen must be achieved in order to properly identify the nodules. On unenhanced MR scans, carcinoid tumours usually appear as isointense to muscle on T_1 weighted images and iso- or mildly hyperintense to muscle on T_2 weighted images [39]. In some cases no discrete mass can be identified and in such cases the tumour usually develops as a focal thickening of the wall of a bowel loop. The most characteristic feature of carcinoid tumours is an intense desmoplastic reaction in the mesentery induced by extraparietal infiltration [14, 40]. Both MDCT and MRI can show an ill-defined soft-tissue mass with irregular margins and infiltrative character related to mesenteric fibrosis (Figure 10). In up to 70% of cases these mesenteric masses contain calcifications that are correctly identified only at MDCT [14]. Moreover, mesenteric calcifications can be used to differentiate carcinoid-induced fibrosis from other conditions such as mesenteric fibromatosis in which calcium precipitation is uncommon [41]. Mesenteric vessel can be involved as a result of direct tumour encasement or desmoplastic reaction. Narrowing

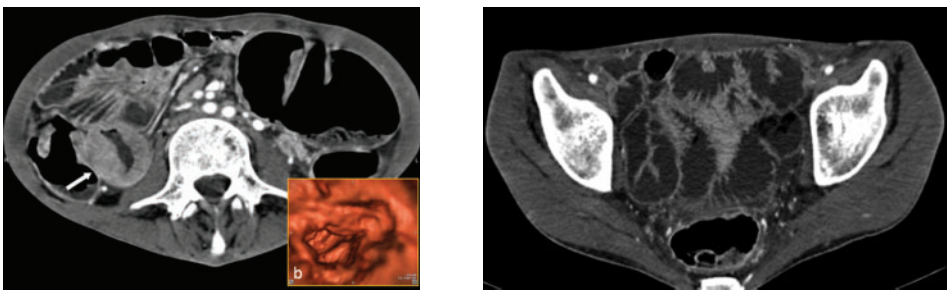

(a) (c)

Figure 11. Atypical carcinoid tumour. 46-year-old female with chronic diarrhoea, flushing, cardiac arrhythmia and high levels of urinary 5-HIAA. (a) Multidetector CT images demonstrate a circumferential thickening of the last ileal loop with sparing of the outer wall layers, (b) some mucosal irregularities can be identified on the retrograde view from virtual endoscopic reconstruction. (c) Caudal sections show marked fluid distension of ileal and jejunal loops owing to carcinoid-induced secretory discharge.

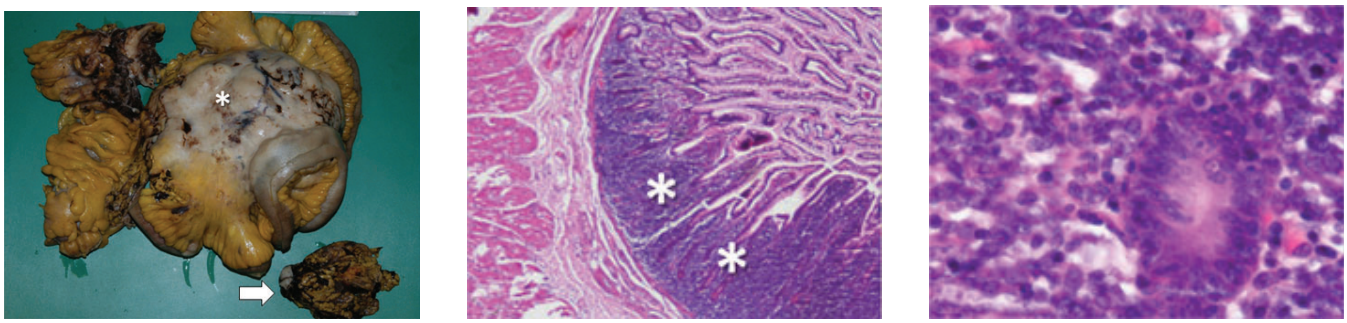

(a) (b) (c)

Figure 12. Non-Hodgkin B-cell lymphoma. (a) Photograph of resected ileal loops and mesentery from a 53-year-old man who presented with abdominal pain and small bowel occlusion shows a bulky, necrotic lymphadenopaty (arrow) and extensive amorphous, neoplastic infiltration of ileal walls and mesentery (asterisk). (b) Low-power photomicrograph (magnification $\times 4$; haematoxylin-eosin stain) demonstrate effacement of mucosa by lymphoid cell infiltrate (asterisk) and adjacent, normal intestinal mucosa. (c) High-power photomicrograph (magnification $\times 400$; haematoxylin–eosin stain) demonstrate large B cells infiltrating glandular crypts.

or engorgement of the vasa recta as well as secretory discharge (Figure 11) can occur owing to the action of hormones secreted by the neoplasm. Special attention should be paid to the identification of synchronous localisations in the SI and to the possible presence of hypervascular liver metastases. Alternative diagnostic modalities such as somatostastin receptor scan or positron emission tomography (PET) with C^{11}-hydroxytrytophan can be a feasible option for suspected carcinoid in the absence of confirmatory conventional cross-sectional imaging data.

Lymphoma

The third most common neoplasm is non-Hodgkin lymphoma (10–15% of cases). This neoplasm is more common in patients with coeliac disease and in patients with acquired immune deficiency syndrome (AIDS), and particularly prevalent in developing countries. Early lesions may appear as plaque-like mucosal expansions while advanced, infiltrating lesions produce full mural thickening and mucosal ulceration. Other lesions may appear as polipoid masses protruding into the lumen. The involvement of the outer layer of the intestinal wall often leads to wide infiltration of the muscularis propria and myenteric plexus, causing motility failure and secondary obstruction [42] (Figure 12). Moreover, the lack of stromal support in larger lesions may determine ischaemia, necrosis and wall perforation. Atypical lymphoid cells populate the superficial epithelium, subsequently replacing the submucosa and even muscle wall in advanced cases (Figure 12). Most SI lymphomas are B cell-type lesions, while a small percentage are T-cell lymphomas, evenly distributed between low- and high-grade lesions [43].

Owing to the proteiform aspects of this neoplasm, small bowel lymphoma has a wide variety of radiological appearances. At least four major patterns of lymphomatous involvement of the SI have been described [14, 44]. The most common type of alteration (50% of cases) is represented by a full-thickness infiltrative lesion with destruction of the normal mucosal folds (Figure 13), which can involve the muscular layer, blocking peristalsis and causing aneurysmal dilatation of the bowel loops. Adenocarcinoma should usually be considered for differential diagnosis, although this lesion typically presents without aneurysmal dilatation of the bowel [14].

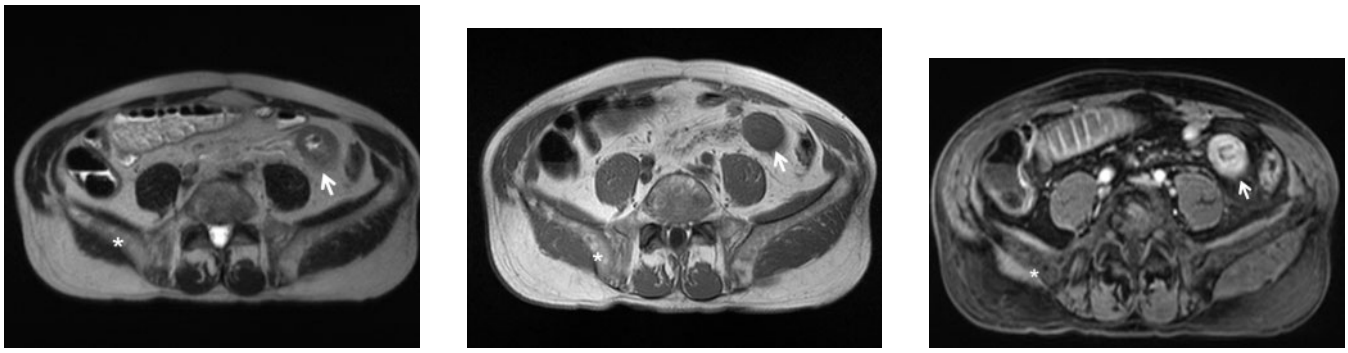

(a) (b) (c)

Figure 13. Lymphoma. 72-year-old female with previously treated non-Hodgkin B-cell lymphoma. (a) Axial T_2 weighted turbo spin echo image demonstrate diffuse wall thickening of one of the last ileal loops (arrow). Signal alteration of the bone marrow of the right iliac wing is also identified (asterisk). (b) T_1 weighted images without and (c) with fat-saturation confirm the findings (arrows), allowing the exclusion of extramural disease. The presence of bone marrow infiltration is well delineated (asterisk) along with a diffuse periosteal enhancement after gadolinium administration.

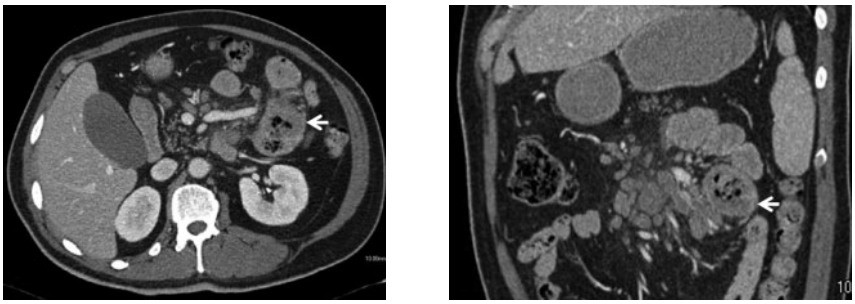

(a) (b)

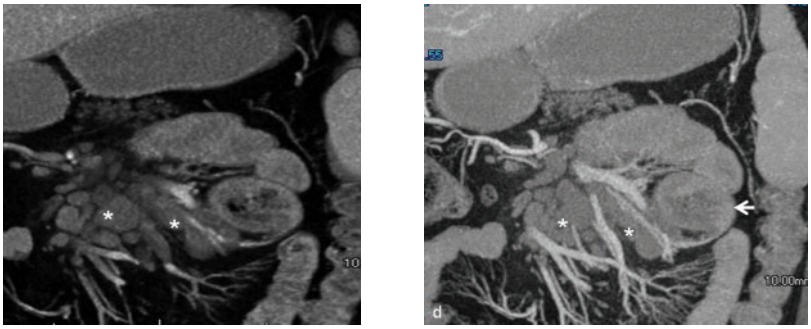

(c) (d)

Figure 14. Lymphoma. Same patient as Figure 12. Multidetector CT images demonstrate a circumferential thickening of (a) the proximal jejunum with mucosal irregularity (arrow) and sparing of the outer wall layers ((b) arrow), bulky lymphadenopaties (asterisk) are identified along the mesenteric vessels.

Lymphoma can also present as multifocal nodules at multiple sites along the SI (requiring differentiation from carcinoid tumour) or as a single mass-forming lesion that may cause intussusceptions or obstruction (Figure 14). Alternatively, an exophytic sarcoma-like form has been described. After contrast agent administration lymphoma demonstrates homogeneous, mild enhancement. Necrosis or fistulous tracts to the adjacent bowel loops have been described, mainly in the exophytic form [45], with increased risk of perforation during chemotherapy. Satellite lymphadenopaties are usually bulky (Figure 14), larger than in other neoplasms and may be used as a differential sign [14].

Gastrointestinal stromal tumours

GI stromal cell tumour (GIST) is the fourth most common SI malignancy, accounting for less than 10% of cases. GISTs develop from the interstitial cells of Cajal, within the Auerbach plexus [46]. Grossly, GISTs appear as rounded, well-defined masses arising from the muscular layer and often developing exophytically or intraluminally, they may be mucosal ulceration present. The size of the lesion may vary from a few millimetres to more than 30 cm. Larger lesions often present central necrosis and haemorrhage (Figure 15). Histologically, GISTs can be classified into spindle cell and epithelioid varieties. The cellular expression of c-kit (CD117), a transmembrane protein receptor with an intracellular tyrosine kinase domain, is typical of GISTs (85–95% of cases) and can be demonstrated with immunohistochemical staining [47] (Figure 15). Epithelioid c-kit negative GISTs usually show early lymphonodal involvement and have a poorer prognosis. The number of mitotic figures per high power-field (HPF) is usually adopted as an empirical cut-off to predict the behaviour of the lesion: 1–5 mitoses per 10

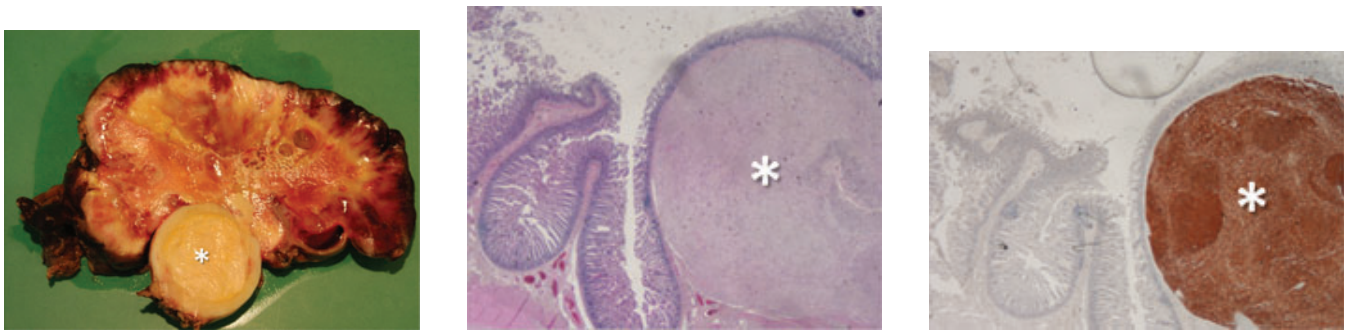

(a) (b) (c)

Figure 15. Gastrointestinal stromal tumour (GIST). (a) Photograph of resected and opened exophytic mass originating from a jejunal loop (not shown) in a 79-year-old woman who presented with abdominal discomfort shows a well-defined inner core (asterisk) surrounded by a larger solid tissue with necrotic and haemorrhagic changes. (b) Low-power photomicrograph (magnification $\times 4$; haematoxylin–eosin stain) of the inner core (asterisk) shows involvement of all submucosal layers without infiltration of the mucosal epithelium. (c) CD-117 antibodies stain confirms GIST diagnosis (asterisk).

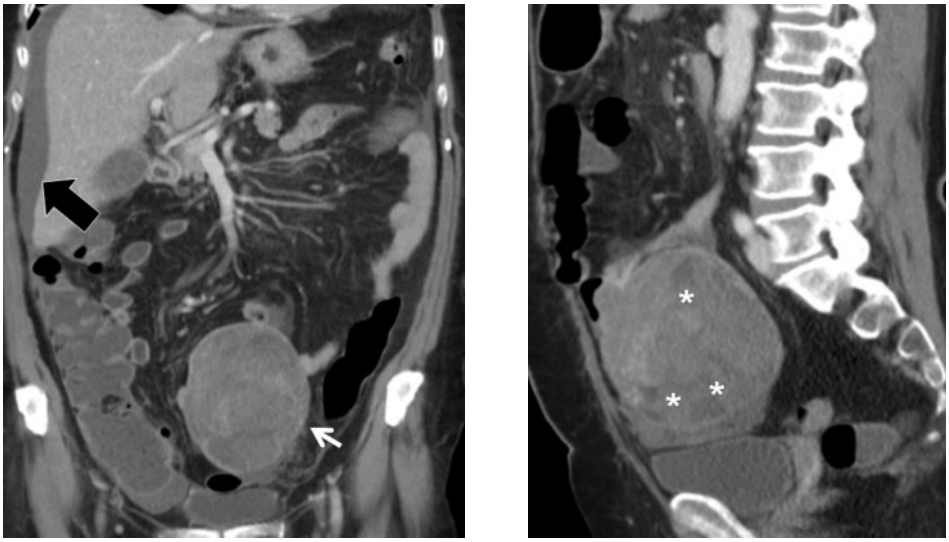

(a) (b)

Figure 16. Low-grade subserosal gastrointestinal stromal tumour (GIST). Same patient as Figure 15. (a) Multidetector CT images demonstrate a large lesion (arrow) with well-defined margins originating from the mesenteric side of one of the last ileal loops, perihepatic ascites is confirmed (black arrow). (b) Sagittal reconstruction clearly demonstrates the prevalent extraluminal extension of the lesion, also evidencing multiple necrotic foci inside the lesion (asterisk).

HPFs suggest potential malignancy, while more than 5 per 10 HPFs indicate malignancy [48]. GISTs occur almost anywhere in the SI, although malignant lesions arise mainly in the distal ileum. GISTs may be classified as:

- submucosal: smooth, round-to-oval filling defect in the SI lumen;
- subserosal: extrinsic or exocentric masses that displace adjacent bowel loops;

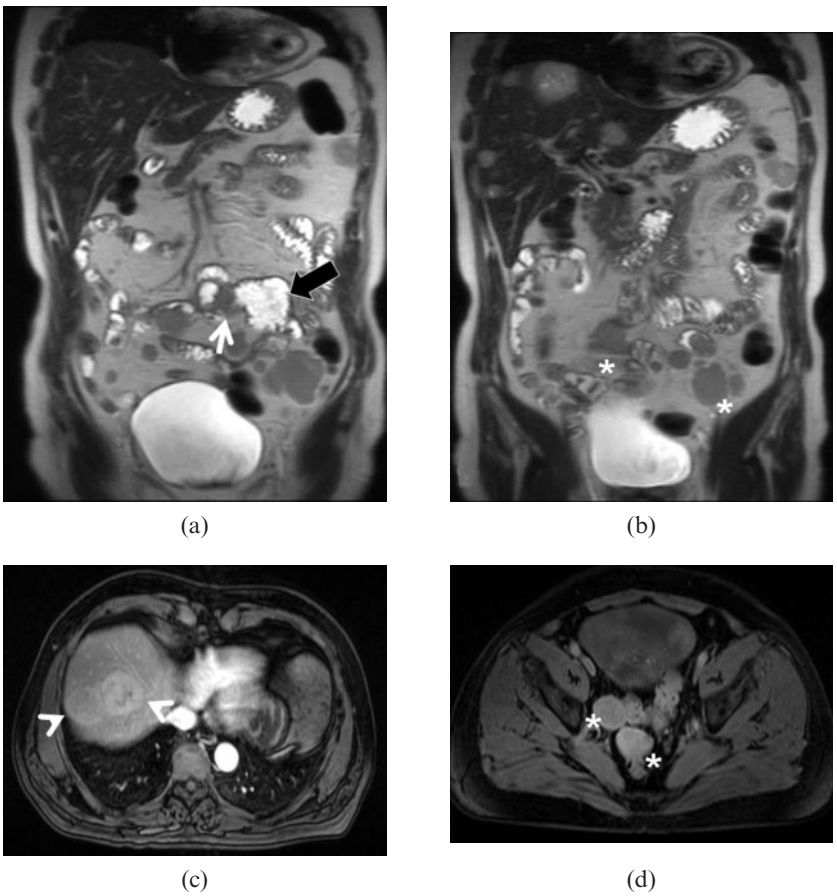

(a) (b)

(c) (d)

Figure 17. High-grade intraluminal gastrointestinal stromal tumour (GIST). 73-year-old female with previously resected GIST and recent onset of intestinal obstruction. (a) Coronal T_2 weighted half-fourier acquisition single shot turbo spin echo image demonstrate a concentric wall thickening at the site of the previous resection (arrow) with dilatation of the upper bowel loop (black arrow). Multiple intestinal and peritoneal implants ((b) asterisk) are also identified. (c) Fat-saturated T_1 weighted spoiled gradient-echo image obtained after intravenous gadolinium administration show hypervascular liver lesions (arrowheads) and pelvic peritoneal implants ((d) asterisk).

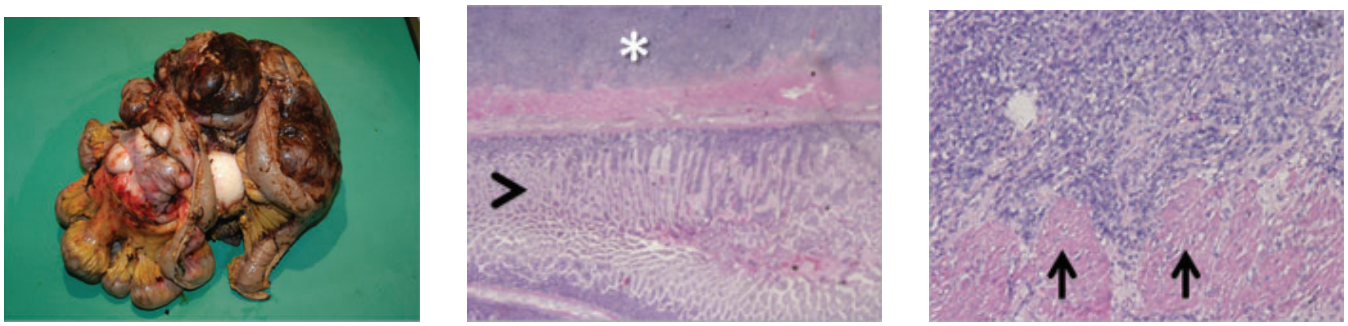

(a) (b) (c)

Figure 18. Metastases. (a) Photograph of resected ileal loops and exophitic masses originating from the bowel wall in a 68-year-old woman with a previous diagnosis of cutaneous melanoma who presented with small bowel occlusion. (b) Low-power photomicrograph (magnification $\times 4$; haematoxylin–eosin stain) shows neoplastic infiltration of the outer layers of bowel wall (asterisk) with intact mucosal epithelium (arrowhead). (c) High-power photomicrograph (magnification $\times 400$; haematoxylin–eosin stain) demonstrate proliferation of round anaplastic cells involving the muscularis propria (arrows).

- intraluminal: hypervascular lesions often correlated with haemorrhage and ulceration.

Other radiological findings that may suggest a malignant form include an irregular shape with low attenuation and internal necrosis on MDCT [49, 50] (Figure 16) and hyperintensity on T_2 weighted MRI indicating central necrosis [16, 51]. Direct spread to adjacent bowel loops, vascular encasement and metastases are common for malignant lesions (Figure 17). Small bowel neurofibromas are similar to benign GISTs and may be equally hypervascular. In patients with acquired immunodeficiency, multiple GISTs must be distinguished from intestinal Kaposi sarcoma [52]. Both MDCT and MRI are important in assessing the response to treatment.

Metastases

Although metastases are the least common SI malignancies, the small bowel remains the main site of metastatic disease in the GI tract. While GISTs, adenocarcinoma and carcinoid tumours often metastasise to the SI, the most frequent extra-abdominal causes of SI metastases are melanoma [53], lung [54], breast and thyroid cancers [55]. Usually macroscopic features such as multifocality, no ulceration and a predominant extramural component may suggest metastatic disease (Figure 18). Histologically, metastases are typically submucosal or subserosal and are easy to distinguish from primary tumours; nevertheless, immunohistochemistry may also help to differentiate primary cancer from metastases (Figure 18). Metastatic spread to the small bowel usually appears as a smooth, round or polypoid mass with the ''target'' aspect of an ulcerated lesion that may result in intussusception or occlusion [22, 56] (Figure 19). Metastases in the small bowel can also occur as extramural nodules following intraperitoneal seeding especially from primary mucinous tumours (ovaries, appendix and colon). An increase in bowel wall thickness with infiltration of the mesenteric fat (omental cake) is the classic radiological feature of intraperitoneal seeding on MDCT and MRI [57]. Since the radiological diagnosis of metastasis is not diagnostic for the primary tumour, a whole body CT scan may be beneficial to reveal the primary site.

Conclusion

Since primary and secondary small bowel neoplasms are rare, present with non-specific symptoms and are small at an early stage, they continue to pose a diagnostic

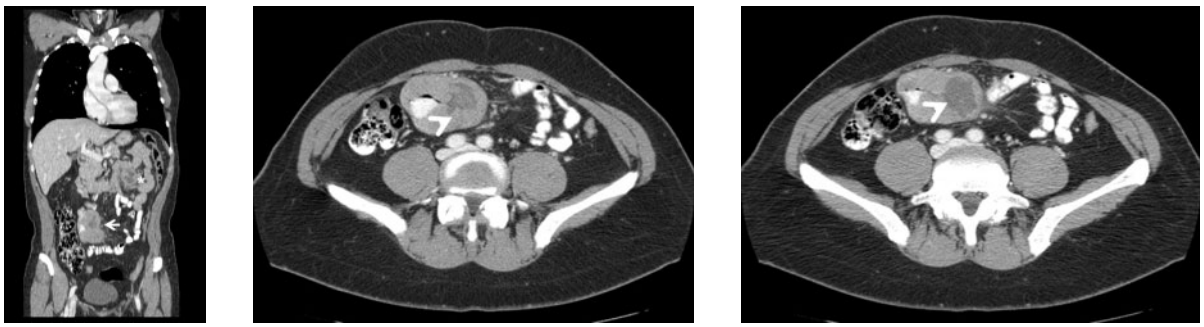

(a) (b) (c)

Figure 19. Metastases (melanoma). Same patient as Figure 18. (a) Multidetector CT images demonstrate a large lesion (arrow), with ill-defined lobulated margins, developing from inner wall layers of an ileal loop, while the lesion develops as a large mass with a necrotic core ((b, c) arrowheads) the bowel is not obstructed for the predominant extramural, vegetating aspect of the tumour.

challenge to radiologists. The use of state of the art MDCT and MRI with appropriate application of tailored scan protocols and an understanding of the imaging signs of each pathological entity, as compared with the natural history of the tumour and microscopic histology, may be of significant help in the daily routine of GI radiologists.

References

1. Martin RG. Malignant tumors of the small intestine. Surg Clin North Am 1986;66:779–85.
2. North JH, Pack MS. Malignant tumors of the small intestine: a review of 144 cases. Am Surg 2000;66:46–51.
3. Horner MJ, Ries LAG, Krapcho M, Neyman N, Aminou R, Howlader N, et al, eds. SEER cancer statistics review, 1975-2006, National Cancer Institute: Bethesda, MD. Available at: http://seer.cancer.gov/csr/1975_2006/
4. Yamagami H, Oshitani N, Hosomi S, Suekane T, Kamata N, Sogawa M, et al. Usefulness of double-balloon endoscopy in the diagnosis of malignant small-bowel tumors. Clin Gastroenterol Hepatol 2008;6:1202–5.
5. Maglinte DD, O'Connor K, Bessette J, Chernish SM, Kelvin FM. The role of the physician in the late diagnosis of primary malignant tumors of the small intestine. Am J Gastroenterol 1991;86:304–8.
6. Nolan DJ, Traill ZC. The current role of barium examination of the small intestine. Clin Radiol 1997;52:809–20.
7. Masselli G, Polettini E, Casciani E, Bertini L, Vecchioli A, Gualdi G. Small-bowel neoplasms: prospective evaluation of MR enteroclysis. Radiology 2009;251:743–50.
8. Maglinte DD, Sandrasegaran K, Lappas JC, Chiorean M. CT Enteroclysis. Radiology 2007;245:661–71.
9. Wold PB, Fletcher JG, Johnson CD, Sandborn WJ. Assessment of small bowel Crohn disease: noninvasive peroral CT enterography compared with other imaging methods and endoscopy — feasibility study. Radiology 2003;229:275–81.
10. Mazzeo S, Caramella D, Battolla L. Crohn disease of the small bowel: spiral CT evaluation after oral hyperhydration with iosotonic solution. J Comput Assist Tomogr 2001;24: 612–16.
11. Winter TC, Ager JD, Nghiem HV, Hill RS, Harrison SD, Freeny PC. Upper gastrointestinal tract and abdomen: water as an orally administered contrast agent for helical CT. Radiology 1996;201:365–70.
12. Megibow AJ, Babb JS, Hecht EM, Cho JJ, Houston C, Boruch MM, et al. Evaluation of bowel distention and bowel wall appearance by using neutral oral contrast agent for multi-detector row CT. Radiology 2006;238:87–95. Erratum in: Radiology 2006;241(3):948.
13. Thompson SE, Raptopoulos V, Sheiman RL, McNicholas MJ, Prassopulos P. Abdominal helical CT: milk as a low-attenuation oral contrast agent. Radiology 1999;211:870–5.
14. Horton KM, Fishman EK. Multidetector-row computed tomography and 3-dimensional computed tomography imaging of small bowel neoplasms: current concept in diagnosis. J Comput Assist Tomogr 2004;28:106–16.
15. Laghi A, Paolantonio P, Passariello R. Small bowel. Magn Reson Imaging Clin N Am 2005;13:331–48.
16. Laghi A, Paolantonio P, Iafrate F, Altomari F, Miglio C, Passariello R. Oral contrast agents for magnetic resonance imaging of the bowel. Top Magn Reson Imaging 2002; 13:389–96.
17. Zhu J, Xu JR, Gong HX, Zhou Y. Updating magnetic resonance imaging of small bowel: imaging protocols and clinical indications. World J Gastroenterol 2008;14:3403–9.
18. Rieber A, Aschoff A, Nussle K, Wruk D, Tomczak R, Reinshagen M, et al. MRI in the diagnosis of small bowel disease: use of positive and negative oral contrast media in combination with enteroclysis. Eur Radiol 2000;10:1377–82.
19. Maccioni F, Bruni A, Viscido A, Colaiacomo MC, Cocco A, Montesani C, et al. MR imaging in patients with Crohn disease: value of T_2- versus T_1-weighted gadolinium-enhanced MR sequences with use of an oral superparamagnetic contrast agent. Radiology 2006;238:517–30.
20. Laghi A, Paolantonio P, Catalano C, Dito L, Carbone I, Barbato M, et al. MR imaging of the small bowel using polyethylene glycol solution as an oral contrast agent in adults and children with celiac disease: preliminary observations. AJR Am J Roentgenol 2003;18:191–4.
21. Laghi A, Carbone I, Catalano C, Iannaccone R, Paolantonio P, Baeli I, et al. Polyethylene glycol solution as an oral contrast agent for MR imaging of the small bowel. AJR Am J Roentgenol 2001;177:1333–4.
22. Sailer J, Zacherl J, Schima W. MDCT of small bowel tumours. Cancer Imaging 2007;7:224–33.
23. Ernst O, Asselah T, Cablan X, Sergent G. Breath-hold fast spin-echo MR imaging of Crohn's disease. AJR Am J Roentgenol 1998;170:127–8.
24. Regan F, Beall DP, Bohlman ME, Khazan R, Sufi A, Schaefer DC. Fast MR imaging and the detection of small-bowel obstruction. AJR Am J Roentgenol 1998;170:1465–9.
25. Lee JK, Marcos HB, Semelka RC. MR imaging of the small bowel using the HASTE sequence. AJR Am J Roentgenol 1998;170:1457–63.
26. Hohl C, Haage P, Krombach GA, Schmidt T, Ahaus M, Günther RW, et al. Diagnostic evaluation of chronic inflammatory intestinal diseases in children and adolescents: MRI with true-FISP as new gold standard? Rofo 2005;177:856–63.
27. Gourtsoyiannis N, Papanikolaou N, Grammatikakis J, Maris T, Prassopoulos P. MR enteroclysis protocol optimization: comparison between 3D FLASH with fat saturation after intravenous gadolinium injection and true FISP sequences. Eur Radiol 2001;11:908–13.
28. Gourtsoyiannis N, Papanikolaou N, Grammatikakis J, Maris T, Prassopoulos P. MR imaging of the small bowel with a true-FISP sequence after enteroclysis with water solution. Invest Radiol 2000;35:707–11.
29. Maccioni F. Double-contrast magnetic resonance imaging of the small and large bowel: effectiveness in the evaluation of inflammatory bowel disease. Abdom Imaging 2010;35: 31–40.
30. Pauls S, Kratzer W, Rieber A, Schmidt SA, Mittrach C, Adler G, et al. Quantifying the inflammatory activity in Crohn's disease using CE dynamic MRI. Rofo 2003;175: 1093–9.
31. Lowenfels AB, Sonni A. Distribution of small bowel tumors. Cancer Lett Jul 1977;3:83–6.
32. Ouriel K, Adams JT. Adenocarcinoma of the small intestine. Am J Surg 1984;147:66–71.
33. Zeh H III. Cancer of the small intestine. In: DeVita VT Jr, Hellman S, Rosenberg SA (eds). Cancer: Principles and Practice of Oncology. 7th ed. Philadelphia, Pa: Lippincott Williams & Wilkins; 2005:1035–48.
34. Bauer RL, Palmer ML, Bauer AM, Nava HR, Douglass HO Jr. Adenocarcinoma of the small intestine: 21-year review of diagnosis, treatment, and prognosis. Ann Surg Oncol 1994;1:183–8.
35. Sata N, Endo K, Shimura K, Koizumi M, Nagai H. A new 3D-diagnosis strategy for duodenal malignant lesions using multi-detector row CT, CT virtual duodenoscopy, duodenography and 3D multi-cholangiography. Abdom Imaging 2007;32:66–72.
36. Kazerooni EA, Quint LE, Francis IR. Duodenal neoplasms: predictive value of CT for determining malignancy and tumor resectability. AJR Am J Roentgenol 1992;159:303–9.
37. Marshall JB, Bodnarchuk G. Carcinoid tumors of the gut. Our experience over three decades and review of the literature. J Clin Gastroenterol 1993;16:123–9.

38. Druce M, Rockall A, Grossman AB. Fibrosis and carcinoid syndrome: from causation to future therapy. Nat Rev Endocrinol 2009;5:276–83.
39. Schmid-Tannwald C, Zech CJ, Panteleon A, Sommer WH, Auernhammer C, Herrmann KA. Characteristic imaging features of carcinoid tumors of the small bowel in MR enteroclysis. Radiologe 2009;49:242–5.
40. Coulier B, Pringot J, Gielen I, Maldague P, Broze B, Ramboux A, et al. Carcinoid tumor of the small intestine: MDCT findings with pathologic correlation. JBR-BTR 2007; 90:507–15.
41. Levy AD, Rimola J, Mehrotra AK, Sobin LH. From the archives of the AFIP: benign fibrous tumors and tumorlike lesions of the mesentery: radiologic-pathologic correlation. Radiographics 2006;26:245–64.
42. Herrmann R, Panahon AM, Barcos MP, Walsh D, Stutzman L. Gastrointestinal involvement in non-Hodgkin's lymphoma. Cancer 1980;46:215–22.
43. Wotherspoon AC. Extragastric MALT lymphoma. Gut 2002;51:148–9.
44. Buckley JA, Jones B, Fishman EK. Small bowel cancer: imaging features and staging. Radiol Clin North Am 1997;35:381–402.
45. Gore RM, Mehta UK, Berlin JW, Rao V, Newmark GM. Diagnosis and staging of small bowel tumours. Cancer Imaging 2006;6:209–12.
46. Koh JS, Trent J, Chen L. Gastrointestinal stromal tumors: overview of pathologic features, molecular biology, and therapy with imatinib mesylate. Histol Histopathol 2004;19: 565–74.
47. Corless CL, Fletcher JA, Heinrich MC. Biology of gastrointestinal stromal tumors. J Clin Oncol 2004;22:3813–25.
48. Demetri GD, Benjamin RS, Blanke CD, Blay JY, Casali P, Choi H, et al. NCCN Task Force Report: management of patients with gastrointestinal stromal tumor (GIST) — update of the NCCN clinical practice guidelines. J Natl Compr Canc Netw 2007;5:S1–S29.
49. Horton KM, Juluru K, Montogomery E, Fishman EK. Computed tomography imaging of gastrointestinal stromal tumors with pathology correlation. J Comput Assist Tomogr 2003;28:811–17.
50. Hong X, Choi H, Loyer EM, Benjamin RS, Trent JC, Charnsangavej C. Gastrointestinal Stromal tumor: role of CT in diagnosis and in response evaluation and surveillance after treatment with Imatinib. Radiographics 2006;26: 481–95.
51. Tateishi U, Miyake M, Maeda T, Arai Y, Seki K, Hasegawa T. CT and MRI findings in KIT-weak or KIT-negative atypical gastrointestinal stromal tumors. Eur Radiol 2006; 16:1537–43.
52. Parfitt JR, Rodriguez-Justo M, Feakins R, Novelli MR. Gastrointestinal Kaposi's sarcoma: CD117 expression and the potential for misdiagnosis as gastrointestinal stromal tumour. Histopathology 2008;52:816–23.
53. Lens M, Bataille V, Krivokapic Z. Melanoma of the small intestine. Lancet Oncol 2009;10:516–21.
54. Kim MS, Kook EH, Ahn SH, Jeon SY, Yoon JH, Han MS, et al. Gastrointestinal metastasis of lung cancer with special emphasis on a long-term survivor after operation. J Cancer Res Clin Oncol 2009;135:297–301.
55. Phillips DL, Benner KG, Keeffe EB, Traweek ST. Isolated metastasis to small bowel from anaplastic thyroid carcinoma. With a review of extra-abdominal malignancies that spread to the bowel. J Clin Gastroenterol 1987;9:563–7.
56. Minordi LM, Vecchioli A, Mirk P, Filigrana E, Poloni G, Bonomo L. Multidetector CT in small-bowel neoplasms. Radiol Med 2007;112:1013–25.
57. Sheth S, Horton KM, Garland MR, Fishman EK. Mesenteric neoplasms: CT appearances of primary and secondary tumors and differential diagnosis. Radiographics 2003;23: 457–73.